Electronic Supplementary Material (ESI) for Energy & Environmental Science.
This journal is © The Royal Society of Chemistry 2014

Supplementary Information for **Semi-transparent Perovskite Solar Cells for Tandems with Silicon and CIGS**

Colin D. Bailie[1†,] M. Greyson Christoforo[2†], Jonathan P. Mailoa[3], Andrea R. Bowring[1], Eva L. Unger[1], William H. Nguyen[4], Julian Burschka[5], Norman Pellet[5], Jungwoo Z. Lee[3], Michael Grätzel[5], Rommel Noufi[6], Tonio Buonassisi[3], Alberto Salleo[2], Michael D. McGehee[1*]

Perovskite Device Procedure:

Pilkington TEC15 FTO glass (1.6 and 2.2mm) was patterned by selective etching with Zn powder (J.T. Baker, 4282-01), 4M HCl (Fisher, A144-212), and mechanical abrasion with a cotton swab. The glass was cleaned by sonication in a diluted Extran solution (EMD, EX0996-1), acetone (EMD, AX0115-1), and isopropanol (IPA) (EMD, PX1835P-4). After 20min of UV-ozone, the glass was heated to 500°C on a hotplate. A 1:10 dilution of titanium diisopropoxide bis(acetylacetonate) (Aldrich - 325252) in ethanol (Sigma-Aldrich, 187380) was repeatedly sprayed from an airbrush nozzle to achieve a ~50 nm thick films of TiO_2 on top of the FTO. After cooling down, the glass was immersed in a 70°C batch of 40 mM $TiCl_4$ (Sigma-Aldrich, 208566) in ultrapure water (J.T. Baker, 6906-02) for 30 min. The glass was then rinsed in DI water and dried on a 70°C hotplate for 15 min. After cooling down, mesoporous TiO_2 films were spun onto the TiO_2/FTO surface at 4000 rpm for 30 s and sintered at 450°C. The spin-coating solution was a 1:3 dilution of 18-NRT TiO_2 paste (Dyesol) in ethanol.

All previous steps were performed in ambient atmosphere. The remainder of device fabrication was performed in a nitrogen glovebox with <5 ppm O_2 and H_2O. The TiO_2 substrates were dried by heating to 500°C with a hot air gun for 30 min and immediately brought into the glovebox. A 1.3 M PbI_2 solution was prepared by dissolving PbI_2 (Aldrich, 211168) into anhydrous DMF (Acros, 32687) and stirring on a hotplate at 100°C. The DMF was filtered through a 200 nm PTFE filter (Pall, 4552) prior to adding to the solution in order to remove particulates. Methylammonium Iodide (MAI) was synthesized according to a previously reported procedure.[1] A solution of 10 mg MAI per 1 mL anhydrous IPA (Acros, 61043) was prepared and allowed to dissolve at room temperature. A pure IPA rinse solution was prepared as well. The IPA was filtered through a 20 nm PTFE filter prior to adding to the solutions in order to remove particulates.

After the TiO_2 substrates were cooled to room temperature, 100 µL of the 100°C PbI_2/DMF solution was pipetted onto the substrate and spun at 6500 rpm for 90 s. The resulting film was translucent yellow and dried for 30 min on a 70°C hotplate. After cooling, the films were dipped in the MAI/IPA solution. The films were monitored optically for the formation of the perovskite (SI Figure X). The signal at 700 nm was used to determine the growth rate of the perovskite, while the signal at 850nm was used to detect the presence of other optical phenomena (changes in scattering, reflection, incident light intensity). When the derivative of both signals matched, the formation was considered complete and the perovskite film was removed, rinsed in IPA, dried by spinning at 4000 rpm for 30 s, and placed back on the 70°C hotplate for 30 min. At this point, the films were a translucent brown. After cooling, 75 µL of a spiro-OMeTAD (Lumtec, LT-S922) solution was spun on top at 4000 rpm for 30 s. The spiro-OMeTAD solution was 59 mM (for opaque devices) and 163 mM spiro-OMeTAD (for semi-transparent devices) in

anhydrous chlorobenzene (Sigma-Aldrich, 284513). The spiro-OMeTAD was dissolved by placing on a hotplate at 70°C for >30 min. 193 mM of tert-butyl pyridine (Aldrich, 142379) and 31 mM of Li-TFSI (Aldrich, 15224) dissolved as 520 mg/mL in anhydrous acetonitrile (Acros, 61096) were added to the 59 mM spiro-OMeTAD solution. For the 163 mM spiro-OMeTAD solution, the amount of tert-butyl pyridine and Li-TFSI was kept consistent with respect to the concentration of the spiro-OMeTAD. In this study, 8 mol% of the spiro-OMeTAD was spiro-OMeTAD$(TFSI)_2$, resulting in 16% of spiro-OMeTAD molecules being chemically oxidized to ensure conductivity in the spiro-OMeTAD layer. The spiro-OMeTAD$(TFSI)_2$ was synthesized as reported elsewhere in literature.[2] After the spiro-OMeTAD solution was prepared, it was filtered through a 20 nm Al2O3 filter (Whatman, 6809-3102) to remove any aggregates and particulates. Films were then removed from the glovebox and stored overnight in a desiccator at 20% RH.

For the opaque electrode devices, 100 nm Au was thermally evaporated through a patterned shadow mask to form the back electrode. For the semi-transparent devices, an AgNW film on PET (details in following section). After transfer of the AgNW electrode, 100 nm Ag was thermally evaporated through a patterned shadow mask around 3 edges of the devices. These bars of silver helped reduce the unnecessary series resistance in the AgNW electrode by not limiting the current collection to one geometrical direction. The nearly completed device was stored in a desiccator for 12 hours before applying the anti-reflective coatings.

LiF anti-reflective coatings were then added to the semi-transparent devices. 133 nm LiF was deposited onto the glass surface. This was optimized to provide anti-reflection for the broad solar spectrum from 400–1100nm. 176 nm LiF was deposited onto the AgNW mesh. This thickness was optimized to provide anti-reflection for the infrared spectrum from 800–1100 nm.

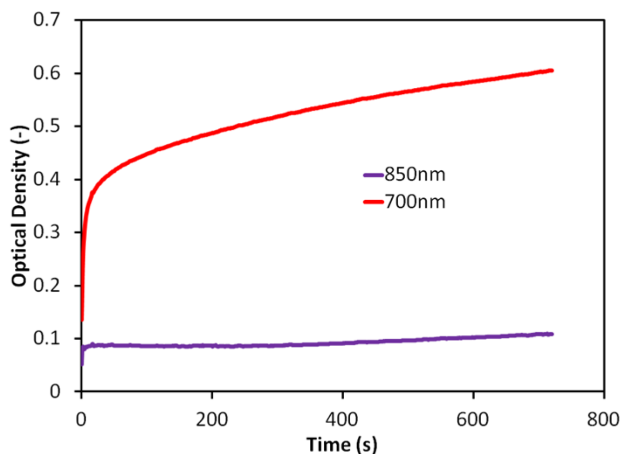

Supplementary Figure 1. Optical density over time of perovskite film in dipping solution. The signal at 700 nm was used to determine the growth rate of the perovskite, while the signal at 850 nm was used to detect the presence of other optical phenomena (changes in scattering, reflection, incident light intensity).

Si Device Procedure:

We fabricate our silicon cells from multicrystalline silicon wafers with high impurity content. Instead of using expensive polysilicon made using the Siemens process, the feedstock for our cast multicrystalline Si wafers are 4.5N (99.995% pure) upgraded metallurgical silicon (UMG-Si) or recycled silicon from the top 10% of a cast multicrystalline industrial ingot (TI-Si). These ~200 µm-thick wafers are subjected to saw-damage removal wet etch in CP4 solution (15:5:2 HNO_3:CH_3COOH:HF) for 2 cycles of 2 minute etch, resulting in ~180 µm thick wafers. The wafers are then cleaned using RCA1 (5:1:1 H_2O:NH_4OH:H_2O_2) and RCA2 (5:1:1 H_2O:HCl:H_2O_2) solutions at 70°C, 10 min. each, to remove organic and metallic surface contaminants. The wafers are then loaded into a Tystar $POCl_3$ diffusion furnace at 700°C for phosphorus emitter formation. After ramping up the furnace temperature to 865°C, $POCl_3$ gas is flowed into the furnace for 12 minutes, followed by 6 minutes of N_2 purge. After waiting for an extra time of 10 minutes, we purge the furnace chamber with O_2 for 7 minutes followed by temperature ramp down of ~ 3°C/minute. The samples are then unloaded at 500°C.

At the end of the diffusion process, phosphorus emitter with diffusion depth of 200–300 nm and emitter sheet resistance of ~35 Ω/□ are formed on both sides of the wafer. We remove the phosphosilicate glass (PSG) layer formed on the wafers surface by dipping them in buffered oxide etch (BOE 5:1) solution for approximately 30 s, then deposit SiN_x anti-reflection coating (ARC) using plasma-enhanced chemical vapor deposition (PECVD). In this intermediate step, the standard Si cells have an ARC thickness of 82 nm, while the cells optimized for infrared light (800–1100 nm) have an ARC thickness of ~125 nm. We remove the backside emitter by SF_6 reactive ion etch (RIE) with a rate of ~1 µm/min to etch ~1 µm deep. After, we deposit 1 µm thick Al on the backside of the wafer using *e*-beam evaporation, followed by rapid thermal annealing (RTA) at 900°C for 30 s in N_2 atmosphere to form aluminum back surface field (Al BSF) at the back of the wafer. After this annealing step, the thickness of the ARC layers shrink down to 78 nm (optimized for standard AM1.5 illumination) and 115 nm (optimized for IR response). We defined our finger area of the cells using photolithography, and etched SiN_x on the corresponding area using RIE. We then deposit 20/20/300 nm Ti/Pd/Ag metal stack as the finger, for which Ti acts as the adhesion layer, Pd acts as the diffusion barrier, and Ag acts as the conductive layer. Lift-off process in acetone is used to form the metal fingers, followed by RTA at 400°C for 5 minutes in Ar atmosphere for metal adhesion. The cells are finally cut out of the wafers by laser scribing followed by mechanical cleaving.

AgNW Spray Deposition

The spray deposition method used here follows that described by Beiley *et al*.[3] with several modifications. The spray nozzle was positioned 76 mm above the substrate. The AgNW dispersion sprayed here contained 4.5 mg of AgNWs. This value was chosen such that the transmission/conductivity tradeoff of the AgNW electrode maximizes the power conversion efficiency of the tandem. The deposition was carried out on 5mil thick Polyethylene terephthalate (PET). The choice of PET as a substrate for the AgNW film is important for the transfer lamination technique for reasons described below. The spray deposition was carried out at the elevated temperature of 60°C to increase the conductivity of the AgNW electrode. PET has a glass transition temperature of about 70°C and so higher deposition temperatures and further annealing, although desirable, could not be used here. The nanowires used here averaged 35 nm in diameter and 15 µm in length.

This spray deposition process yielded a 50 × 300 mm of AgNW transparent electrode on PET. This was then cut with scissors into pieces approximately matching the perovskite substrate size. The electrodes were patterned by selectively applying and then removing kapton tape to eliminate AgNWs in desired regions. The AgNW film on PET was stored at ambient laboratory conditions for two weeks before transfer lamination.

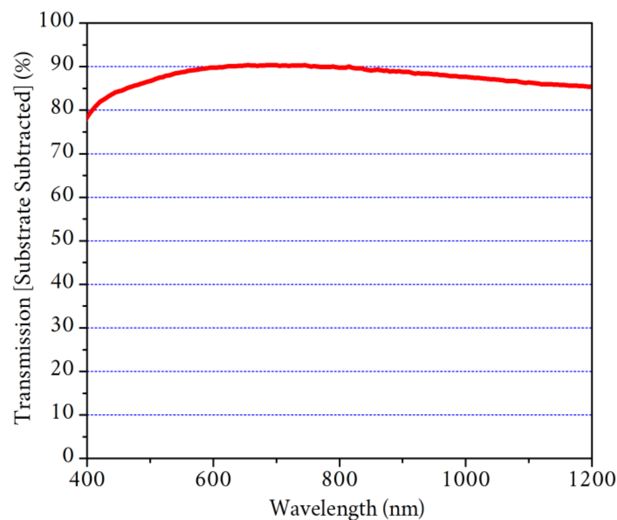

Supplementary Figure 2. Transmission of the 12.4 Ω/□ AgNW film with the PET substrate subtracted.

AgNW Transfer Lamination

Please see Supplementary Movie 1 for a demonstration of this process.

The patterned AgNW film on PET was placed facedown onto the nearly completed perovskite device so that the AgNWs were in contact with the top spiro-OMeTAD layer. A 0.17 mm thick glass coverslip was placed on top of the PET substrate. The AgNWs were transfer laminated from the PET to the perovskite solar cell by applying approximately 500g of downward force onto the coverslip through a single ¼-inch diameter ball bearing. The bearing was selectively rolled over the active area of the perovskite device so that the AgNW film is completely and uniformly donated from the PET to the top spiro-OMeTAD layer of the perovskite solar cell. The rolling action of the bearing reduces lateral shear force on the PET preventing any movement of the donor PET substrate relative to the acceptor perovskite solar cell. Lateral movement here causes discontinuities in the laminated AgNW film severely degrading its conductivity. The flexibility and softness of the PET substrate allows the AgNW film to conform to the surface of the perovskite device during transfer despite any dust or other imperfections that may be present on either the surface of the AgNW film or the surface of the spiro-OMeTAD layer. This, coupled with the relatively small contact point of the ball bearing ensures complete transfer lamination of the AgNW film to the perovskite device without damaging the mechanically sensitive nanostructured AgNW film in the presence of dust or other imperfections.

The 500 g transfer force was chosen to be sufficient to ensure the AgNWs were completely donated from the PET but not too much that they were forced through the spiro-OMeTAD layer causing bridges/shunts across it. AgNW bridges across the spiro-OMeTAD layer lead to increased recombination since the spiro-OMeTAD layer can no longer effectively block electrons and in extreme cases shunting of the device if the AgNWs bridge through the TiO_2 as well. The coverslip serves two purposes. First, it isolates the lateral movement of the ball bearing from the PET, which prevents cracks, or discontinuities in the transferred AgNW film as described above. Second, it serves to increase the area over which the force from the ball bearing is applied to the PET, thus reducing the pressure felt by the AgNWs during the transfer process. This reduced pressure is a further safeguard against AgNWs bridging through the spiro-OMeTAD layer.

<u>Tips For Reproduction:</u>

For those with interest towards reproducing this work, we would like to stress a few points in our procedure above that we have found to be the most critical in fabricating the semi-transparent perovskite devices.

- Avoid a perovskite overlayer and make the spiro-OMeTAD layer thick. Planarization of the top surface is important for ensuring the complete transfer of the silver nanowire electrode. To a lesser degree, it also improves the transmission through the device by decreasing scattering.
- Transfer the silver nanowires with as little pressure as possible. A very low and consistent pressure is required to avoid pressing the wires through the spiro-OMeTAD film and making direct contact with the perovskite. This is also the function served by the glass coverslip.

- Develop a surface coating on the wires to make them more stable. Our laboratory environment has normal oxygen levels as well as a small partial pressure of sulfur gas added to the environment. While we have no direct proof of a coating on the silver nanowires, we believe either an oxide or a sulfide layer was formed on the surface of the wires. Silver oxide and sulfide are much more stable than metallic silver in the presence of iodine (which readily forms silver iodide) and improve the resistance of the electrode to corrosion. We see that electrodes stored in the laboratory environment prior to transfer onto a device are much more stable than electrodes stored in an inert nitrogen atmosphere. We set aside one of these devices for long-term testing and it showed no change in performance over a month of storing in the dark in desiccated air. There is certainly room to improve on this procedure by intentionally introducing an oxide or sulfide layer onto the nanowires or by coating the surface with other materials (*e.g.*,. ligands, a gold coating, *etc*.)
- Wait for the spiro-OMeTAD layer to dry before transfer. Possibly the spiro-OMeTAD film is too soft while still wet. Our results were much more inconsistent and lower when we tried transfer onto a wet spiro-OMeTAD layer. We achieved our best results by allowing the device to dry overnight in a flow desiccator.
- Test devices before evaporating anti-reflection coatings. The LiF anti-reflection coating seems to act as an effective seal against ingress of gas. For us, however, perovskite devices need to be exposed to light and oxygen to achieve their best performance (we believe the necessity is in the perovskite layer itself, not the spiro-OMeTAD layer), otherwise there is a slight s-kink near max power. Testing in the middle of fabrication gets rid of this s-kink permanently, then the anti-reflection coating can be added.

Device Variability

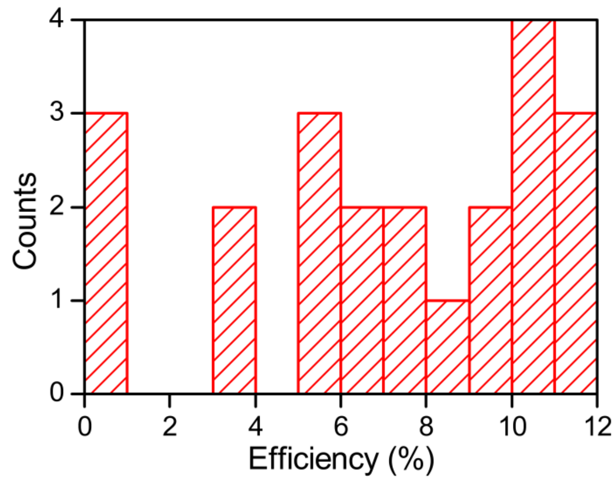

Supplementary Figure 3. Distribution of semi-transparent cell performance gathered from 3 batches where device procedures were largely kept constant between batches. Low-efficiency devices exhibited shorting likely caused by too much pressure applied manually during the AgNW electrode transfer. Medium-efficiency devices generally exhibited low photocurrents likely caused by incomplete transfer of the AgNW electrode due to too little pressure applied manually during the electrode transfer.

Testing Procedures:

EQE Measurements:

For the perovskites, the external quantum efficiency (EQE) was recorded as a function of the wavelength using a Model SR830 DSP Lock-In Amplifier (Stanford Research Systems) without light bias. A 100 W tungsten lamp (Newport) was used to provide an excitation beam, which was focused through a Princeton Instruments SpectraPro 150 monochromator and chopped at approximately 2 Hz. At each wavelength, a delay time of 3 s was used to allow the signal to settle, and afterwards data was collected for 4 s. The time constant on the lock-in amplifier was 1 s.

For the Si and CIGS cells, the EQE measurement was sped up because these cells have much faster settling times than the perovskites. The excitation beam was chopped at 300Hz, the delay time was reduced to 0.1 s, data was collected for 1 s, and the time constant of the lock-in amplifier was 30 ms.

To measure the EQE of the bottom cell in the tandem, the above procedure for the Si and CIGS cells was repeated with the perovskite top cell placed in front of the Si or CIGS cell to filter the incoming light. The EQE and IV measurements were made immediately following the evaporation of the LiF anti-reflective coatings.

4-Point Probe and Transmission: Measurements:

Sheet resistance and transmission measurements were performed as previously described in the supplemental section of Beiley *et al*. (2013).[3]

NREL Certification:

Stanford

Perovskite filtered CdS/Cu(In,Ga)(S,Se) Cell

Device ID: best 2
May 09, 2014 13:08
Spectrum: ASTM G173 global

Device Temperature: 25.0 ± 0.5 °C
Device Area: 0.3896 cm^2
Irradiance: 1000.0 W/m^2

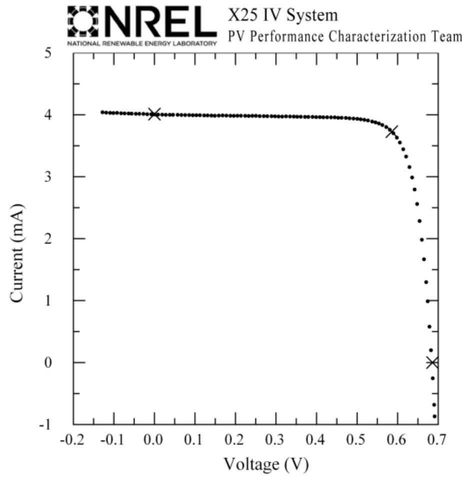

V_{oc} = 0.6859 V
I_{sc} = 4.0100 mA
J_{sc} = 10.293 mA/cm^2
Fill Factor = 79.39 %

I_{max} = 3.7277 mA
V_{max} = 0.5858 V
P_{max} = 2.1835 mW
Efficiency = 5.60 %

Stanford

semi-transparent Perovskite Cell

Device ID: Device A
May 09, 2014 10:20
Spectrum: ASTM G173 global

Device Area: 0.3896 cm^2
Irradiance: 1000.0 W/m^2

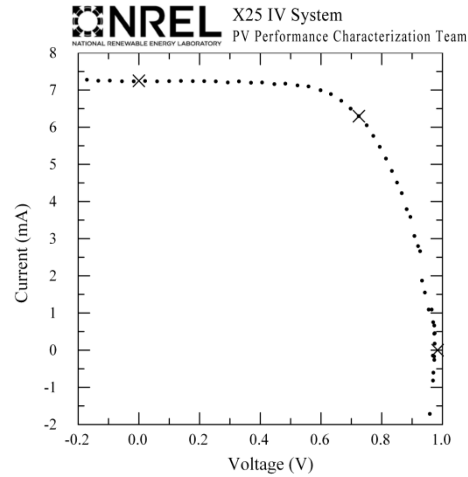

V_{oc} = 0.9843 V
I_{sc} = 7.2457 mA
J_{sc} = 18.598 mA/cm^2
Fill Factor = 63.95 %

I_{max} = 6.2960 mA
V_{max} = 0.7244 V
P_{max} = 4.5607 mW
Efficiency = 11.71 %

Supplementary Figure 4: A non-champion cell was sent to NREL for certification. The tandem efficiency as measured in-house at Stanford was 17.1%. The certified tandem efficiency was even slightly higher at 5.6% + 11.7% = 17.3%. The difference in efficiency measurements can be explained by sensitivity of the NREL EQE to 300-800nm, whereas in-house EQE was only measured to 350-800nm

NREL Certification cont'd:

Stanford University

mono-Si Cell

Device ID: 15517-15
Oct 16, 2014 14:47
Spectrum: ASTM G173 global

Device Temperature: 24.8 ± 0.5 °C
Device Area: 0.3906 cm^2
Irradiance: 1000.0 W/ m^2

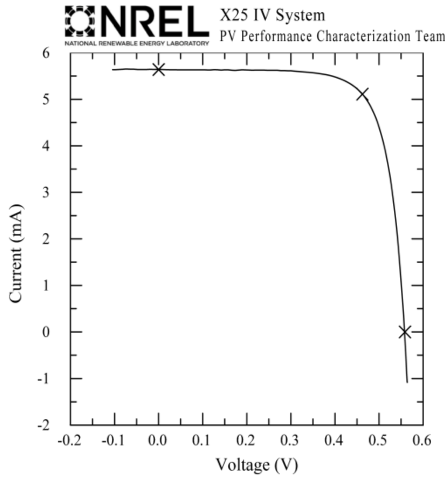

V_{oc} = 0.5589 V
I_{sc} = 5.6369 mA
J_{sc} = 14.432 mA/cm^2
Fill Factor = 74.97 %

I_{max} = 5.1081 mA
V_{max} = 0.4624 V
P_{max} = 2.3618 mW
Efficiency = 6.05 %

Stanford University

Perovskite Cell

Device ID: 1001
Oct 14, 2014 10:14
Spectrum: ASTM G173 global

Device Temperature: 26.8 ± 2.7 °C
Device Area: 0.3906 cm^2
Irradiance: 1000.0 W/ m^2

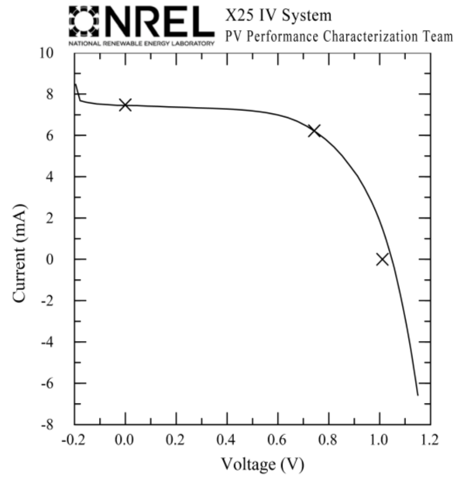

V_{oc} = 1.0111 V
I_{sc} = 7.4783 mA
J_{sc} = 19.146 mA/cm^2
Fill Factor = 61.08 %

I_{max} = 6.2185 mA
V_{max} = 0.7426 V
P_{max} = 4.6181 mW
Efficiency = 11.82 %

Supplementary Figure 5: A tandem certified at NREL with a semi-transparent perovskite top cell and a 17%-alone mono-Si bottom cell. The tandem efficiency is 6.1% + 11.8% = 17.9%

Full TI-Si Results:

We chose to use two different Si devices to illustrate how re-optimization of the bottom cell specifically for use in a tandem can improve the tandem efficiency. One Si device uses the broad-spectrum AR coating while the other has an AR coating optimized for the infrared (IR-ARC). In main text, the TI-Si with a broadband AR coating was used as the single-junction baseline and the TI-Si with an IR-ARC was filtered by the perovskite and added to the perovskite efficiency to arrive at the tandem performance.

Supplementary Table 1: Cell characteristics of TI-Si solar cells and their corresponding tandem performance.

Cell	J_{SC} (mA/cm^2)	V_{OC} (mV)	*FF* (-)	Efficiency (%)	Tandem Efficiency (%)
Perovskite	17.5	1025	0.710	12.7	
TI-Si	29.3	582	0.667	11.4	
TI-Si Filtered	10.7	539	0.648	3.7	16.4
TI-Si + IR-ARC	28.0	593	0.712	11.8	
TI-Si + IR-ARC Filtered	11.1	547	0.704	4.3	17.0

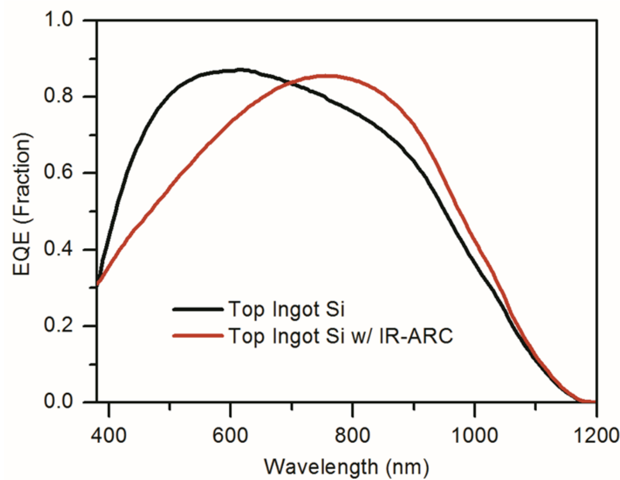

Supplementary Figure 6. Example of difference in spectral response depending on AR coating applied to Si cell. The regular TI-Si cell has a broadband AR coating.

UMG-Si Results:

Supplementary Table 2: Cell characteristics of UMG-Si solar cell not shown in main text and its corresponding tandem performance.

Cell	J_{SC} (mA/cm^2)	V_{OC} (mV)	*FF* (-)	Efficiency (%)	Tandem Efficiency (%)
Perovskite	17.5	1025	0.710	12.7	
UMG-Si	27.9	590	0.705	11.6	
UMG-Si Filtered	9.4	553	0.698	3.6	16.3

References

1. M. M. Lee, J. Teuscher, T. Miyasaka, T. N. Murakami, and H. J. Snaith, *Science (New York, N.Y.)*, 2012, **338**, 643–647.

2. W. H. Nguyen, C. D. Bailie, E. L. Unger, and M. D. Mcgehee, *J. Am. Chem. Soc.*, 2014, **136**, 10996–11001.

3. Z. M. Beiley, M. G. Christoforo, P. Gratia, A. R. Bowring, P. Eberspacher, G. Y. Margulis, C. Cabanetos, P. M. Beaujuge, A. Salleo, and M. D. McGehee, *Advanced materials (Deerfield Beach, Fla.)*, 2013, **25**, 7020–6.